Eur. J. Mineral., 36, 641–656, 2024
https://doi.org/10.5194/ejm-36-641-2024

European Journal of Mineralogy
Open Access

Lazerckerite, $Ag_{3.75}Pb_{4.5}(Sb_{7.75}Bi_4)S_{24}$, from Kutná Hora, Czech Republic: a new Sb–Bi member of the andorite branch of the lillianite homologous series

Richard Pažout[1], **Michal Dušek**[2], **Jiří Sejkora**[3], **Jakub Plášil**[2], **Gheorghe Ilinca**[4], and **Zdeněk Dolníček**[3]

[1]University of Chemistry and Technology Prague, Technická 5, 166 28, Praha 6, Czech Republic
[2]Institute of Physics of the Czech Academy of Sciences, Cukrovarnická 10/112, Praha, Czech Republic
[3]Department of Mineralogy and Petrology, National Museum, Cirkusová 1740, 193 00, Praha 9, Czech Republic
[4]Department of Geology, Mineralogy and Paleontology, University of Bucharest, Bd. N. Balcescu, 1, 010041 Bucharest, Romania

Correspondence: Richard Pažout (richard.pazout@vscht.cz)

Received: 5 December 2023 – Revised: 27 May 2024 – Accepted: 14 June 2024 – Published: 28 August 2024

Abstract. Lazerckerite, ideally $Ag_{3.75}Pb_{4.5}(Sb_{7.75}Bi_4)S_{24}$, is a new mineral species found in medieval mine dumps of the historic Ag–Pb–Zn Kutná Hora ore district, Czech Republic. The mineral is associated with other Sb–Bi lillianite homologues (terrywallaceite, gustavite, holubite) and Ag,Bi-bearing galena, most frequently as grain aggregates and replacement rims of earlier Ag–Pb–Bi minerals, growing together in aggregates of up to 0.6×0.3 mm. Lazerckerite is opaque, is steel grey in colour, and has a metallic lustre; the calculated density is $5.920\,\mathrm{g\,cm^{-3}}$. In reflected light lazerckerite is greyish white, and bireflectance and pleochroism are weak with grey tints. Anisotropy is weak to moderate with grey to bluish-grey rotation tints. Internal reflections are not observed. Electron microprobe analyses yielded the empirical formula, based on 44 apfu, $(Ag_{3.61}Cu_{0.04})_{\Sigma 3.65}(Pb_{4.55}Fe_{0.01}Cd_{0.01})_{\Sigma 4.57}(Sb_{7.87}Bi_{3.75})_{\Sigma 11.62}(S_{24.15}Se_{0.01})_{\Sigma 24.16}$. Its unit cell parameters are $a = 13.2083(9)$, $b = 19.4595(8)$, $c = 8.4048(13)$, $\beta = 90.032(7)°$, $V = 2160.3(4)$ Å^3, space group $P2_1/c$, and $Z = 2$. The structure of lazerckerite contains two Pb sites (Pb1 and Pb2) in bicapped trigonal prismatic coordination, 8 independent octahedral sites, and 13 distinct sulfur positions. Four of the octahedral sites are mixed (Sb,Bi) and (Bi,Sb) sites, one is a mixed (Ag,Bi) site, and one is a mixed (Sb,Pb) site. The new mineral belongs to the andorite branch of the lillianite homologous series with $N = 4$ and is a new addition to the group of Sb–Bi mixed members of the series. Lazerckerite is defined as a lillianite homologue with the three following requirements: $N = 4$, L ($Ag^+ + (Bi^{3+}, Sb^{3+}) \leftrightarrow 2\,Pb^{2+}$ substitution) $\approx 90\,\%$–$95\,\%$, and approximately one-third of atom percentage of antimony is replaced by bismuth ($Bi/(Bi+Sb) \approx 0.30$–0.38). The new mineral has been approved by the Commission on New Minerals, Nomenclature and Classification (CNMNC) of the International Mineralogical Association (IMA 2022-113) and named after Lazarus Ercker, the supreme Royal Bergmeister of the Kingdom of Bohemia and the Master of Prague Mint.

1 Introduction

A new sulfosalt mineral species, lazerckerite, ideally $Ag_{3.75}Pb_{4.5}(Sb_{7.75}Bi_4)S_{24}$, has been found in medieval mine dumps of the Staročeské pásmo Lode of the historic Kutná Hora Ag–Pb–Zn ore district, Central Bohemia, Czech Republic (Fig. 1). The mineral is named after Lazarus Ercker (1528–1594), the supreme Royal Bergmeister of the Kingdom of Bohemia (Minister of Mining) and the Master of Prague Mint, a renowned metallurgist, chemist, and mining specialist and the author of the *Books on Assaying* (original title *Beschreibung Allerfürnemisten Mineralischen Ertzt und Berckwercksarten*). This work – published in 1574 – was reissued 15 times, translated into four languages, and until the end of the 18th century was used as a principal textbook by all mining universities and Bergakademie in Europe. The pronunciation of the mineral name is "lazerke'rait". The new mineral and its name have been approved by the Commission on New Minerals, Nomenclature and Classification (CNMNC) of the International Mineralogical Association (IMA 2022-113) (Pažout et al., 2023b). Holotype material of lazerckerite (polished section) is deposited in the collections of the Department of Mineralogy and Petrology, National Museum in Prague, Cirkusová 1740, 19300 Praha 9, Czech Republic, under the catalogue number P1P 11/2022.

Lazerckerite is a new member of the lillianite group of natural sulfosalts of Ag–Pb–(Sb,Bi,As). The last comprehensive review of both lillianite (Bi-rich) and andorite (Sb-rich) branches of the lillianite homologous series was conducted by Makovicky and Topa (2014). A general overview of Sb–Bi mixed members was given in Topa at al. (2016). Lazerckerite belongs to the andorite branch of the lillianite homologous series, and it is a new addition to the fairly new group of Sb–Bi mixed members of the series, which up to date is comprised of five minerals: terrywallaceite (lillianite branch; Yang et al., 2013), oscarkempffite (andorite branch; Topa et al., 2016), clino-oscarkempffite (andorite branch; Makovicky et al., 2017), staročeskéite (lillianite branch; Pažout and Sejkora, 2018), and holubite (andorite branch; Pažout et al., 2023a).

This paper describes the sixth Sb–Bi member of the series, lazerckerite; its physical and chemical properties; its crystal structure; and its relation to other lillianite homologues.

2 Occurrence and mineral association

Lazerckerite was found in 21 different samples in gangue material of the medieval mine dumps of the Staročeské pásmo Lode (the Old Bohemian Lode in English) of the historic Kutná Hora Ag–Pb–Zn ore district. Kutná Hora is a hydrothermal-vein-type deposit of Variscan age (Holub et al., 1982), mined mainly between the 14th and 17th centuries with 10 major lodes (zones) (Fig. 1), with each lode consisting of several principal veins (Pažout et al., 2017). From the point of view of geology and mineralogy, two min-

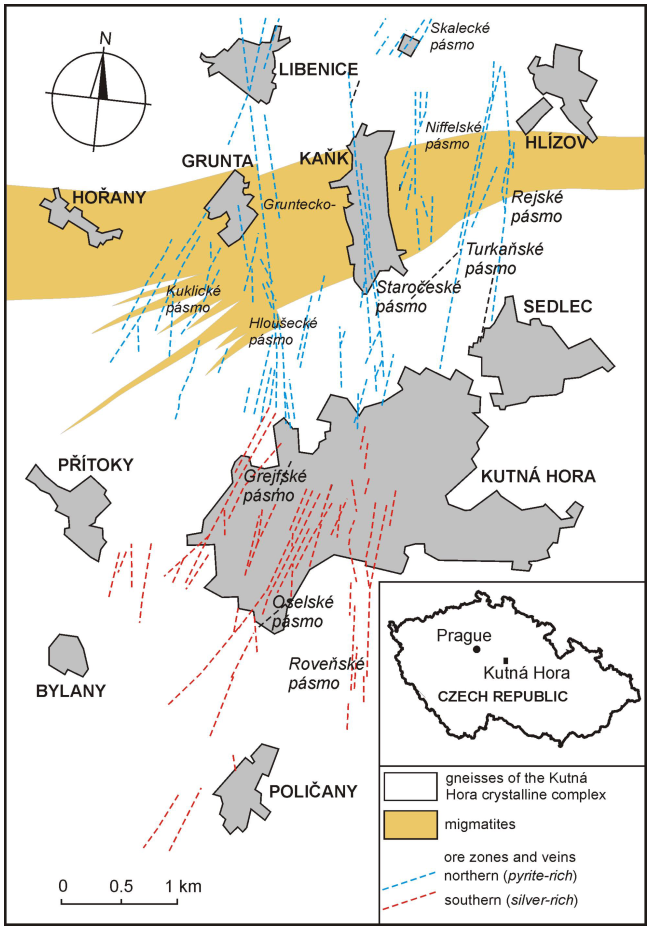

Figure 1. Map of Kutná Hora ore district with major lodes (zones) (Malec and Pauliš, 1997).

eral assemblages are distinguished in this ore district, one "silver-rich" in the southern part of the ore district and one "pyrite-rich" in the northern part (Malec and Pauliš, 1997). The Staročeské pásmo Lode belongs to the northern pyrite-rich lodes, and it is the biggest lode of the Kutná Hora ore district, both in terms of the amount of extracted ore and the amount of extracted silver (estimated 300 t of Ag). The full list of minerals (over 150 species) recorded from this area is given at http://www.mindat.org/loc-18419.html, last access: 30 July 2024.

In the holotype sample (ST 48), lazerckerite forms grains in association with terrywallaceite, Bi-rich jamesonite, and remnants of Ag,Bi-bearing galena (Fig. 2). The hand specimen is formed by limonite-coloured quartz with silvery-grey metallic grains of the above Bi-bearing minerals up to 3 × 3 mm. The quartz gangue of the holotype sample contains grains and lenses of pyrrhotite several millimetres in size, with no other base sulfides present.

In most other samples, the mineral occurs frequently as replacement rims of earlier Ag–Pb–Bi–Sb minerals and grain aggregates, growing together in aggregates up to 0.6 ×

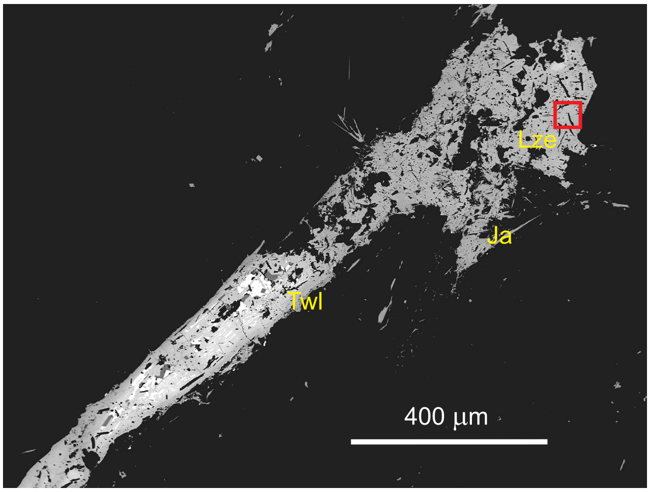

Figure 2. A grain of lazerckerite (Lze) with needles of Bi-rich jamesonite (Ja) on the edges. The bottom-left part of the grain is formed by terrywallaceite (Twl) with remnants of Ag,Bi-bearing galena (white), which is being replaced by terrywallaceite. The red box indicates the area where the grain used for single-crystal X-ray diffraction was extracted. BSE image of the holotype sample ST 48.

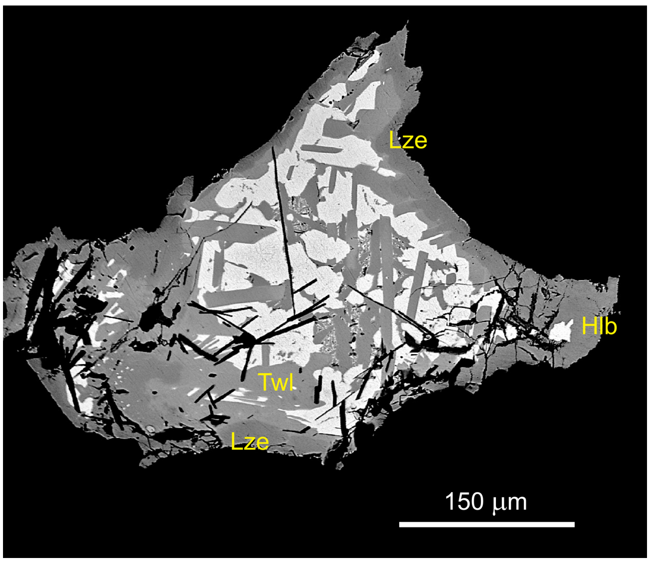

Figure 3. A frequent association of mixed Sb–Bi members of the lillianite homologous series with $N = 4$ from Kutná Hora ore district, Czech Republic: Ag,Bi-bearing galena (white) replaced by lamellae of terrywallaceite (Twl) and replacement rims of holubite (Hlb) and lazerckerite (Lze, darker than Hlb). The succession is galena → terrywallaceite → holubite → lazerckerite. BSE image of sample ST 29.

0.3 mm. It often occurs in close association with Ag,Bi-bearing galena, terrywallaceite, and holubite, occasionally accompanied by other lillianite homologues. In Fig. 3 Ag,Bi-bearing galena is being replaced by terrywallaceite, and the replacement rims are formed by holubite, which is subsequently replaced by lazerckerite (darker than holubite in backscatter electron (BSE) images due to significantly lower Pb content).

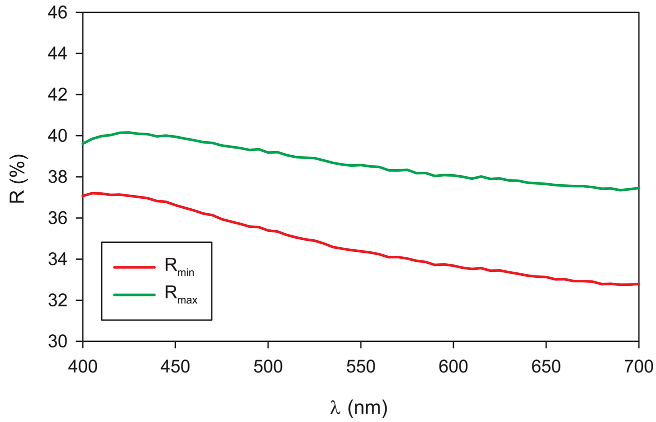

Figure 4. Reflectance curve for lazerckerite from Kutná Hora.

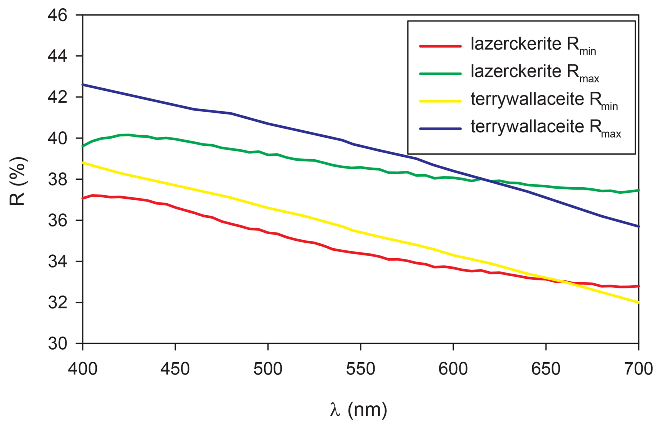

Figure 5. The comparison of lazerckerite reflectance curves with the curves for terrywallaceite from Mina Herminia, Julcani Mining District, Huancavelica, Peru (Yang et al., 2013); staročeskéite from Kutná Hora (Pažout and Sejkora, 2018); and holubite from Kutná Hora (Pažout et al., 2023a).

The origin of the mineral is related to the later Bi mineralization, and we assume the mineral is a replacement product of earlier, Bi-richer lillianite homologues and galena that crystallized from originally low-temperature (ca. 100–250 °C) hydrothermal fluids in the tectonically opened fractures in yet earlier hydrothermal Fe–Cu–Zn–Sn–As base sulfide ore vein fillings (Pažout and Sejkora, 2018). Lazerckerite is one of the latest in the Bi sulfosalt mineralization stage, following the usual sequence of crystallization in the Kutná Hora ore district: native Bi → galena ss → matildite → izoklakeite/cosalite → eskimoite/treasurite/vikingite → gustavite → Sb-rich gustavite → staročeskéite/terrywallaceite → holubite → lazerckerite → Bi-rich jamesonite (Pažout and Sejkora, 2018). A general succession trend observed in

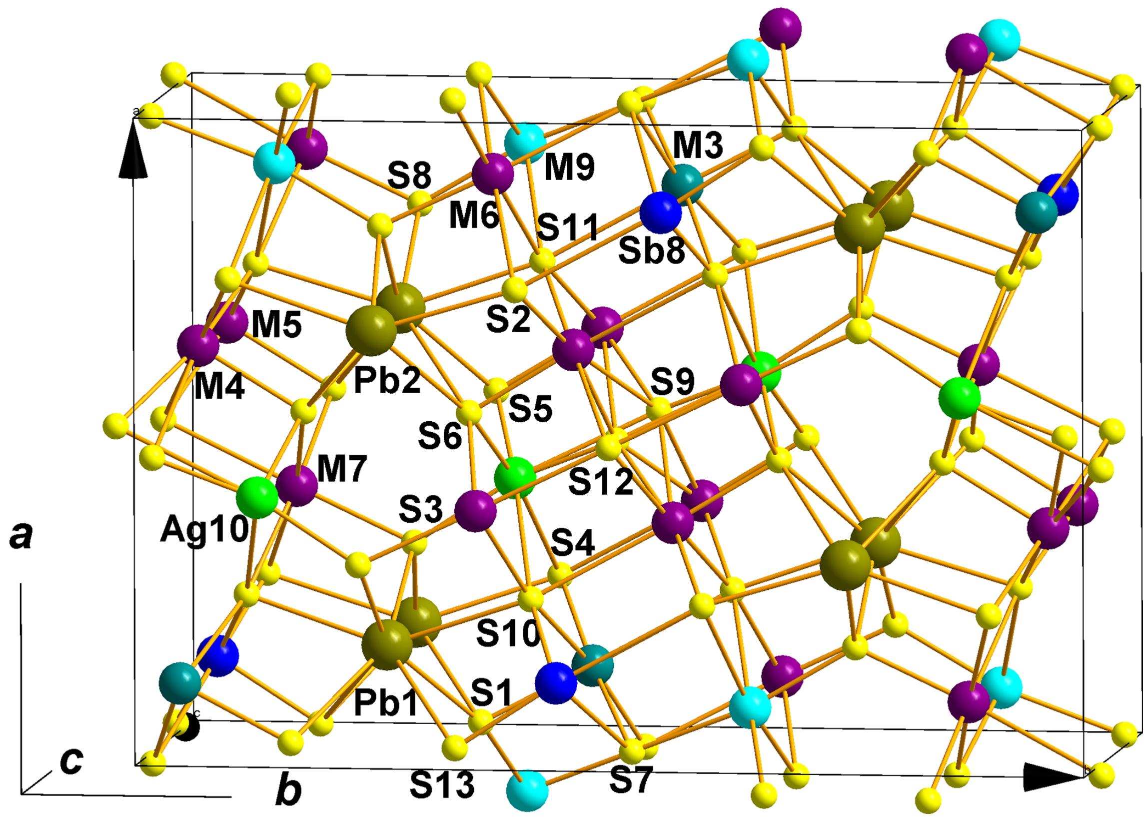

Figure 6. Cation and anion sites in the crystal structure of lazerckerite, a natural Sb–Bi $^{4,4}L$ homologue of the lillianite homologous series. Pb1 and Pb2 are lead atoms in bicapped trigonal prismatic coordination (CN 8); all other metal atoms are in octahedral coordination (CN 6). Marginal octahedra are Ag10, $M7$ ((Bi,Sb) mixed site), $M6$ ((Bi,Sb) mixed site), and $M9$ ((Ag,Bi) mixed site). Central octahedra are $M4$ ((Sb,Bi) mixed site), $M5$ ((Sb,Bi) mixed site), Sb8, and $M3$ ((Sb,Pb) mixed site). View along c axis.

Table 1. Reflectance values of lazerckerite (COM standard wavelengths are given in bold).

$R_{min.}$	$R_{max.}$	λ (nm)	$R_{min.}$	$R_{max.}$	λ (nm)
37.1	39.6	400	34.2	38.5	560
37.1	40.1	420	33.9	38.2	580
36.8	40.0	440	**33.7**	**38.0**	**589**
36.4	39.8	460	33.7	38.1	600
36.1	**39.6**	**470**	33.4	37.9	620
35.8	39.5	480	33.2	37.7	640
35.4	39-2	500	**33.1**	**37.7**	**650**
35.0	38.9	520	33.0	37.6	660
34.5	38.6	540	32.8	37.4	680
34.4	**38.6**	**546**	32.8	37.5	700

Table 2. Chemical data for lazerckerite ($n = 5$).

Constituent	wt %	Range	Estimated SD
Ag	10.12	9.96–10.38	0.14
Cu	0.06	0.00–0.10	0.04
Fe	0.02	0.00–0.05	0.02
Pb	24.48	23.92–25.21	0.42
Cd	0.02	0.00–0.07	0.03
Sb	24.91	23.93–25.30	0.26
Bi	20.38	19.63–21.02	0.57
Se	0.02	0.00–0.10	0.03
S	20.12	19.88–20.37	0.14
Total	100.13	99.33–100.99	0.71

the Ag–Pb–Bi–Sb mineralization in Kutná Hora ore district is from Bi-dominant to Sb-dominant mineral phases.

3 Physical and optical properties

Lazerckerite is opaque, is lead grey in colour, and has a metallic lustre and grey streak. Cleavage was not observed. The calculated density equals 5.920 g cm^{-3} on the basis of the empirical formula, 5.960 g cm^{-3} on the basis of the ideal formula, and 6.001 g cm^{-3} on the basis of the structural formula, all with single-crystal unit cell parameters. In reflected light lazerckerite is greyish white, and bireflectance and pleochroism are weak with grey tints. Anisotropy is weak to moderate, with grey to bluish-grey rotation tints. Fluores-

Table 3. Calculated X-ray powder diffraction data for lazerckerite. Intensity and d_{hkl} were calculated using the software Diamond 4 (Putz and Brandenburg, 2017) on the basis of our single-crystal structure refinement. Only reflections with $I_{calc}>3$ are listed. The eight strongest reflections are given in bold.

h	k	l	d_{calc}	I_{calc}	h	k	l	d_{calc}	I_{calc}
−2	1	0	6.2538	4	3	−8	2	1.8991	9
−2	2	0	5.4643	6	2	−4	4	1.8513	3
−2	4	0	3.9169	15	−5	6	2	1.8415	5
−1	−2	2	3.7037	18	5	−6	2	1.8409	5
1	−2	2	3.7027	16	−6	6	0	1.8214	3
−1	**−3**	**2**	**3.4079**	**32**	−4	9	0	1.8089	6
1	**−3**	**2**	**3.4071**	**34**	−2	−5	4	1.7807	18
−2	**5**	**0**	**3.3530**	**100**	2	−5	4	1.7803	16
4	0	0	3.3021	20	−4	0	4	1.7732	5
−4	1	0	3.2555	19	4	0	4	1.7723	4
0	6	0	3.2432	4	−4	−1	4	1.7659	4
1	−4	2	3.0915	3	4	−1	4	1.7650	4
−3	**−1**	**2**	**3.0043**	**22**	−3	−9	2	1.7621	3
3	**−1**	**2**	**3.0027**	**25**	3	−9	2	1.7618	4
−2	6	0	2.9111	18	−7	1	2	1.7150	4
−3	**−2**	**2**	**2.9023**	**39**	7	−1	2	1.7143	4
3	**−2**	**2**	**2.9009**	**37**	−2	11	0	1.7088	3
−3	−3	2	2.7532	17	2	−6	4	1.7036	3
3	−3	2	2.7520	16	−4	10	0	1.6765	9
−2	7	0	2.5622	3	−8	1	0	1.6451	5
0	8	0	2.4324	3	−8	2	0	1.6278	6
−1	−7	2	2.2837	9	−6	−4	4	1.4512	6
1	−7	2	2.2835	10	6	−4	4	1.4504	5
−4	7	0	2.1266	4	0	−10	4	1.4277	9
−5	3	2	2.1148	9	−1	−13	2	1.4022	5
5	−3	2	2.1139	8	1	−13	2	1.4021	5
0	**0**	**4**	**2.1012**	**29**	−7	9	2	1.3469	3
−6	3	0	2.0846	3	7	−9	2	1.3465	3
−1	−8	2	2.0791	18	−3	−2	6	1.3227	3
1	−8	2	2.0789	17	−4	−10	4	1.3107	4
−5	4	2	2.0325	15	4	−10	4	1.3103	3
5	−4	2	2.0316	16	−9	5	2	1.3055	4
−6	4	0	2.0056	17	9	−5	2	1.3051	4
0	10	0	1.9459	11	−10	3	0	1.2943	3
−6	5	0	1.9161	7	−2	15	0	1.2730	3
−3	−8	2	1.8995	9	−1	−8	6	1.2089	3

cence and internal reflections were not observed. Reflectance values of lazerckerite, measured in air (WTiC Zeiss 370 standard, MSP400 Tidas spectrophotometer at Leica microscope, objective 50×) are in Table 1 and Fig. 4. The comparison of reflectance curves of lazerckerite, terrywallaceite, holubite, and staročeskéite is given in Fig. 5.

4 Chemical composition

Chemical analyses of the holotype sample were performed using a JEOL JXA-8600 electron probe microanalyser of the University of Salzburg in WDS mode (25 kV, 35 nA) and with a beam diameter of 5 µm. The following standards and X-ray lines were used: $CuFeS_2$ (Cu$K\alpha$, Fe$K\alpha$), Ag (Ag$L\alpha$), PbS (Pb$L\alpha$), Bi_2S_3 (Bi$L\alpha$, S$K\alpha$), Sb_2S_3 (Sb$L\alpha$), CdTe (Cd$L\beta$, Te$L\alpha$), Bi_2Te_2S (Bi$L\alpha$, Te$L\alpha$), and Bi_2Se_3 (Se$K\alpha$). Raw data were corrected with an online ZAF-4 procedure. A second set of polished sections with lazerckerite was measured on a CAMECA SX100 electron probe microanalyser at the National Museum, Prague. The analytical conditions were as follows: WDS mode; accelerating voltage of 25 kV; beam current of 20 nA; electron-beam diameter of 2 µm; and the standards chalcopyrite (S$K\alpha$), Bi_2Se_3 (Bi$M\beta$), PbS (Pb$M\alpha$), Ag (Ag$L\alpha$), halite (Cl$K\alpha$), Sb_2S_3 (Sb$L\alpha$), CdTe (Cd$L\alpha$), HgTe (Hg$M\alpha$), pyrite (Fe$K\alpha$), Cu (Cu$K\alpha$), ZnS (Zn$K\alpha$), NiAs (As$L\beta$), and PbSe (Se$L\beta$). Peak counting time is 20 s for each element and 10 s for each background, and the detection limits for the four trace elements (Cu, Fe, Cd, and Se) were in the range 0.03 wt %–0.06 wt %. Measured data were corrected using PAP software (Pouchou and Pichoir, 1985). Analytical data for the holotype sample are given in Table 2. Its empirical formula (calculated on the basis of 44 apfu) is represented by grouping the constituents according to valence state: $(Ag_{3.61}Cu_{0.04})_{\Sigma 3.65}(Pb_{4.55}Fe_{0.01}Cd_{0.01})_{\Sigma 4.57}$ $(Sb_{7.87}Bi_{3.75})_{\Sigma 11.62}(S_{24.15}Se_{0.01})_{\Sigma 24.16}$.

The simplified formula is $(Ag,Cu)_{3.7}(Pb,Fe,Cd)_{4.6}$ $(Sb_{7.9}Bi_{3.8})_{\Sigma 11.7}S_{24}$, and the ideal formula is $Ag_{3.75}Pb_{4.50}(Sb_{7.75}Bi_4)S_{24}$, which requires Ag 10.47, Pb 24.13, Sb 25.21, Bi 20.28, and S 19.92 weight percentages, totalling 100.00 wt %, corresponding to $N_{chem} = 4.00$, $L\% = 93.75$, and $Bi/(Bi+Sb) = 0.34$. Lazerckerite can be differentiated from chemical results from similar Sb–Bi mixed members of the lillianite homologous series on the basis of $L\%$ (the percentage of the $(Ag + (Bi,Sb) = 2Pb)$ substitution and the Bi : Sb ratio expressed as $Bi/(Bi+Sb)$ (both calculated from electron probe microanalyser (EPMA) results).

5 Crystallography and crystal structure

A tiny fragment of lazerckerite with dimensions of $0.040 \times 0.040 \times 0.035$ mm was extracted from a polished section of the holotype sample and separated under the optical stereomicroscope. The intensity data were collected at ambient temperature using an Oxford Diffraction Gemini single-crystal diffractometer equipped with SuperNova CCD detector and using monochromated Mo$K\alpha$ radiation from a conventional sealed X-ray tube (55 kV, 30 mA), collimated with a fibre-optic Mo-enhanced collimator. A total of 25 883 reflections were measured. After averaging, 5189 reflections were independent and 2750 classified as observed $[I_{obs} > 3\sigma(I)]$. Data were corrected for background, Lorentz, and polarization effects, and a multi-scan correction for absorption was applied, resulting in R_{int} of the merged data equal to 0.0852. The twinning tool incorporated in the Jana2020 program (Petříček et al., 2023) revealed the crystal is twinned on (001) in this unit cell orientation and the volume fractions of each twin is 0.548(5) and 0.452(5). The final refinement of occupancies returned values close to those obtained from the microprobe study. Refinement for 146 parameters converged to the final $R = 0.1063$ and $wR = 0.1876$ for 2750 observed reflections with goodness of fit (GOF) = 2.10 for all reflections.

In the process of indexing, a monoclinic cell was found; images from data collection revealed a primitive unit cell with the presence of reflections doubling the size of the shortest sulfosalt parameter (c in this setting), typical of fizelyite, ramdohrite, and oscakempffite. The unit cell parameters determined from single-crystal data by a least-squares algorithm using the CrysAlisPro Package (Rigaku, 2019) are as follows: $a = 13.2083(9)$, $b = 19.4595(8)$, $c = 8.4048(13)$, $\beta = 90.032(7)°$, $V = 2160.3(4)$ Å^3, space group $P2_1/c$, and $Z = 2$. The powder X-ray diffraction data could not be collected due to the paucity of material; the calculated powder diffraction data are given in Table 3.

Table 4. Summary of data collection conditions and refinement parameters for lazerckerite.

Crystal data	
Structural formula	$Ag_{3.65}Pb_{4.72}Sb_{7.42}Bi_{4.11}S_{24}$
Crystal system	monoclinic
Space group	$P2_1/c$ (no. 14)
a (Å)	13.2083(9)
b (Å)	19.4595(8)
c (Å)	8.4048(13)
β	90.032(7)
V (Å^3)	2160.3(4)
Z	2
Density (calc.) (g cm^{-3})	6.001
$F(000)$	3324
Crystal size (mm)	$0.040 \times 0.040 \times 0.035$
Crystal colour	metallic grey
Data collection	
Temperature	ambient
Diffractometer	Oxford Diffraction Gemini
Radiation	Mo$K\alpha$ 55 kV, 30 mA
Number of frames	670
Measurement time (s per frame)	250
R_{int}	0.0839
Measured reflections	26345
Unique reflections	5189
Observed reflections ($I > 3\sigma(I)$)	2750
$\theta_{min}/\theta_{max}$	2.6/28.57
Range of h, k, l	$h(min) = -17$, $h(max) = 17$ $k(min) = -25$, $k(max) = 25$ $l(min) = -11$, $l(max) = 11$
Refinement	
Refinement on	F^2
R, wR (observed reflections)	0.1063/0.1876
R, wR (all reflections)	0.1769/0.2050
GOF (observed reflections)	2.651
GOF (all reflections)	2.097
No. of least-squares parameters	146
No. of constraints	55
Largest difference peak/hole (e.Å^{-3})	3.67/−3.11*

* This value is for sin(th)/lambda limit set to 0.5 (corresponding to $d = 1$ Å).

The structure of lazerckerite was solved using the charge-flipping algorithm (Palatinus and Chapuis, 2007) implemented in the Jana2020 program (Petříček et al., 2023). Systematic absences and intensity statistics indicated the centrosymmetric space group $P2_1/c$. All atomic positions were found, which were subsequently refined by full-matrix least squares based on F^2 using Jana2020 (Petříček et al., 2023). The distance and bond valence calculations indicated that the trigonal prismatic sites Pb1 and Pb2 are occupied solely by Pb, similarly to other known structures of lillianite homologues with $N = 4$ and $L \leq 100\,\%$. Interatomic dis-

Table 5. Fractional atomic coordinates, occupancies, and equivalent isotropic displacement factors.

Site		SoF	x/a	y/b	z/c	Ueq/iso [Å^2]
Pb1			0.17355(18)	0.25029(15)	0.2560(4)	0.0631(9)
Pb2			0.67635(12)	0.25038(10)	1.0023(4)	0.0330(6)
$M3$	Sb	0.640(13)	1.12840(15)	0.45199(11)	0.4954(4)	0.0271(8)
	Pb	0.360(13)	1.12840(15)	0.45199(11)	0.4954(4)	0.0271(8)
$M4$	Sb	0.623(15)	0.63198(18)	0.05234(15)	0.2509(4)	0.0402(11)
	Bi	0.377(15)	0.63198(18)	0.05234(15)	0.2509(4)	0.0402(11)
$M5$	Sb	0.577(14)	0.36697(16)	−0.05207(13)	0.2497(4)	0.0331(9)
	Bi	0.423(14)	0.36697(16)	−0.05207(13)	0.2497(4)	0.0331(9)
$M6$	Sb	0.487(15)	0.90290(17)	0.13636(13)	0.7500(3)	0.0330(8)
	Bi	0.513(15)	0.90290(17)	0.13636(13)	0.7500(3)	0.0330(8)
$M7$	Sb	0.382(13)	0.39992(19)	0.14029(11)	0.5016(4)	0.0399(8)
	Bi	0.618(13)	0.39992(19)	0.14029(11)	0.5016(4)	0.0399(8)
Sb8			1.13536(17)	0.44375(14)	1.0044(5)	0.0273(10)
$M9$	Ag	0.825(14)	0.9158(3)	0.3669(3)	0.7516(6)	0.069(2)
	Bi	0.125(14)	0.9158(3)	0.3669(3)	0.7516(6)	0.069(2)
Ag10			0.4160(3)	0.37058(19)	0.5029(6)	0.0433(14)
S1			1.0397(8)	0.3349(6)	0.4830(19)	0.043(3)
S2			0.7424(9)	0.0981(6)	0.497(2)	0.045(3)
S3			0.3145(8)	0.2640(6)	0.498(2)	0.036(3)
S4			1.2462(8)	0.3998(6)	0.7938(14)	0.027(3)
S5			0.5334(7)	0.3362(6)	0.7430(17)	0.026(3)
S6			0.4671(9)	−0.1629(7)	0.2394(18)	0.040(3)
S7			0.9890(8)	0.4940(6)	0.7092(11)	0.024(2)
S8			0.8202(7)	0.2557(6)	0.753(2)	0.026(2)
S10			1.2499(8)	0.4042(6)	1.2154(13)	0.021(3)
S11			0.2475(9)	−0.0997(7)	0.004(2)	0.055(4)
S13			1.0325(8)	0.3363(6)	1.0136(18)	0.037(3)
S12			0.5	0	0.5	0.0317 2
S9		0.5	0.4780(16)	0.4792(12)	0.472(3)	0.034(6)

Table 6. Anisotropic displacement parameters with estimated standard uncertainties in parentheses.

Site	U_{11}	U_{22}	U_{33}	U_{12}	U_{13}	U_{23}
Pb1	0.0720(15)	0.0639(16)	0.0535(16)	0.0004(15)	−0.030(2)	−0.0050(13)
Pb2	0.0227(7)	0.0338(10)	0.0425(12)	−0.0007(8)	−0.0063(14)	−0.0030(11)
M3	0.0204(12)	0.0172(12)	0.0436(17)	−0.0034(9)	−0.0008(15)	0.0207(14)
M4	0.0373(17)	0.047(2)	0.0360(18)	−0.0018(14)	−0.0206(17)	0.0096(16)
M5	0.0285(14)	0.0299(16)	0.0410(17)	−0.0114(11)	−0.0115(16)	0.0070(14)
M6	0.0204(11)	0.0435(16)	0.0351(15)	0.0090(12)	−0.0022(14)	−0.0132(14)
M7	0.0321(11)	0.0332(13)	0.0544(17)	−0.0171(10)	−0.0058(17)	0.0060(15)
Sb8	0.0109(12)	0.0282(16)	0.043(2)	−0.0032(11)	0.0008(18)	0.0306(19)
M9	0.071(4)	0.071(4)	0.066(3)	−0.043(3)	−0.022(3)	0.042(3)
Ag10	0.043(2)	0.047(2)	0.040(2)	−0.0260(17)	−0.018(2)	−0.019(2)

tances showed that two central octahedral, as well as two marginal octahedral (i.e. positioned at the margin of the ^4L octahedral slab bordering on the Pb trigonal prism), are in fact (Sb,Bi) mixed sites, which was confirmed by the difference Fourier and refinement results in Jana2020 and charge density calculations in the program ECON21 (Ilinca, 2022). It also showed that the marginal octahedral $M9$ site is a mixed position ($0.835Ag + 0.125Bi$) and that the $M3$ position is in fact a mixed site with ($0.64Sb + 0.36Pb$). For all mixed sites, the coordinates and atomic displacement parameters were kept identical. All metal atoms were refined with anisotropic atomic displacement parameters, and isotropic displacement parameters were used for sulfur. Details of data collection, crystallographic data, and refinement are given in Table 4. Atom coordinates, occupancies, and isotropic displacement parameters are in Table 5; anisotropic atomic

Table 7. Selected interatomic distances (Å).

Pb1	S3	2.7704(3)	M4	S5	2.5297(1)	Sb8	S4	2.4511(2)
	S3	2.8719(3)		S2	2.6852(3)		S10	2.4544(2)
	S1	3.0783(2)		S9	2.7624(2)		S13	2.4953(1)
	S4	3.0909(1)		S11	2.8222(3)		S7	3.1553(3)
	S10	3.1795(1)		S12	2.9089(3)		S7	3.2936(3)
	S13	3.2271(3)		S9	3.1655(3)		S2	3.4101(1)
	S13	3.3158(3)		S10	3.2896(1)	M9	S8	2.5045(1)
	S1	3.3368(3)	M5	S6	2.5306(1)		S7	2.6811(1)
Pb2	S8	2.8273(3)		S2	2.7214(3)		S13	2.7542(3)
	S8	2.8426(3)		S11	2.7600(3)		S1	2.8579(3)
	S2	3.0751(1)		S9	2.8323(3)		S11	3.1117(3)
	S11	3.1011(1)		S12	2.9224(3)		S2	3.1580(3)
	S5	3.2399(3)		S9	3.1034(3)	Ag10	S9	2.2820(1)
	S6	3.2578(3)		S4	3.3855(1)		S3	2.4693(1)
	S5	3.3322(3)	M6	S8	2.5659(1)		S5	2.6311(3)
	S6	3.3385(3)		S13	2.6761(3)		S6	2.6379(3)
M3	S7	2.5428(2)		S1	2.7224(3)		S9	3.2484(1)
	S1	2.5639(1)		S11	2.9557(3)		S10	3.3294(3)
	S7	2.6995(3)		S2	3.0925(3)		S4	3.3668(4)
	S10	2.9963(3)		S7	3.1352(1)			
	S4	3.1207(4)	M7	S3	2.6595(1)			
	S11	3.2771(1)		S4	2.7901(3)			
				S10	2.8121(3)			
				S6	2.8320(3)			
				S5	2.8359(3)			
				S12	3.0331(1)			

displacement parameters in Table 6; and interatomic distances in Table 7. The crystallographic information files have been deposited with the *European Journal Of Mineralogy* and are available in the Supplement (see below). The final structural formula is $Ag_{3.65}Pb_{4.72}Sb_{7.42}Bi_{4.11}S_{24}$, which is in acceptable agreement with the microprobe-established composition $(Ag_{3.61}Cu_{0.04})_{\Sigma 3.65}(Pb_{4.55}Fe_{0.01}Cd_{0.01})_{\Sigma 4.57}(Sb_{7.87}Bi_{3.75})_{\Sigma 11.62}(S_{24.15}Se_{0.01})_{\Sigma 24.16}$. The empirical formula showing site populations represented by the results of the structure determination is ${}^{Ag10}(Ag_2)$ ${}^{M9}(Ag_{1.61}Bi_{0.22})_{\Sigma 1.83}$ ${}^{Pb(1,2)}(Pb_4)$ ${}^{M3}(Pb_{0.54}Sb_{1.46})_{\Sigma 2.00}$ ${}^{M4}(Sb_{1.36}Bi_{0.64})_{\Sigma 2.00}$ ${}^{M5}(Sb_{1.23}Bi_{0.77})_{\Sigma 2.00}$ ${}^{M6}(Sb_{0.97}Bi_{1.03})_{\Sigma 2.00}$ ${}^{M7}(Sb_{0.85}Bi_{1.09})_{\Sigma 1.95}$ ${}^{Sb8}(Sb_2)$ S_{24}.

The structure of lazerckerite, a natural Sb–Bi monoclinic ${}^{4,4}L$ homologue of the lillianite homologous series, contains 10 cation (metal) sites and 13 anion (sulfur) sites. The metal sites consist of two Pb sites (Pb1 and Pb2) in bicapped trigonal prismatic coordination and eight independent octahedral sites. Four of the octahedral sites are marginal octahedra – two of them ($M6$ and $M9$) flanking the trigonal prism of Pb1 and the other two ($M7$ and Ag10) flanking the bicapped trigonal prism of Pb2 – and four ($M3$ and Sb8; $M4$ and $M5$) are central octahedra inside the ${}^4L$ slabs. Both types of octahedra (marginal and central) can be viewed as being formed by one row (or column) along c, each row consisting of two alternating metal sites. The structure of lazerckerite projected down [001] is depicted in Fig. 6.

With regard to the marginal octahedra, in one row (column) the Ag site Ag10 alternates with the (Sb,Bi) mixed site $M7$ (0.62Bi + 0.38Sb), and in the other row the (Ag,Bi) mixed site $M9$ (0.825Ag + 0.125Bi) alternates with the (Bi,Sb) mixed site $M6$ (0.51Bi + 0.49Sb).

6 Site populations and distortion of the coordination polyhedra

The analysis of site populations within the crystal structure of lazerckerite can be enhanced by examining the distortion of the coordination polyhedra expressed by various parameters such as the state of opposing bond pairs, average bond distances, and the departure (EDEV) of ECoN (effective coordination number) from the constrained coordination number (i.e. determined by the ligands with non-zero weight bonds with respect to the charge distribution; Ilinca, 2022). Opposing "in-plane" and "out-of-plane" bond pairs may be analysed in relation to element-specific bond-length hyperbolae, as detailed by Trömel (1980) and Berlepsch et al. (2001a, b). Each bond pair consists of a shorter and an opposite longer connection between the central atom and its ligands. In coordination octahedra, the in-plane bond distances are situated within the common base of the square pyramids. In contrast,

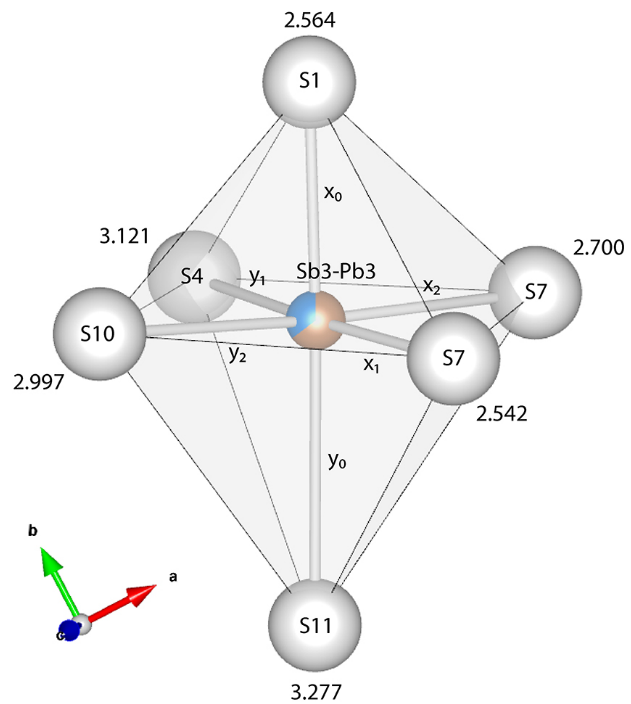

Figure 7. The in-plane (x_1–y_1, x_2–y_2) and the out-of-plane (x_0–y_0) bond pairs in the coordination octahedron of Sb3–Pb3. Stronger interactions are noted with x_0, x_1, and x_2 and the weaker ones with y_0, y_1, and y_2. Bond distances [Å] are shown near each ligand. Figure 7 was created with VESTA (Momma and Izumi, 2011).

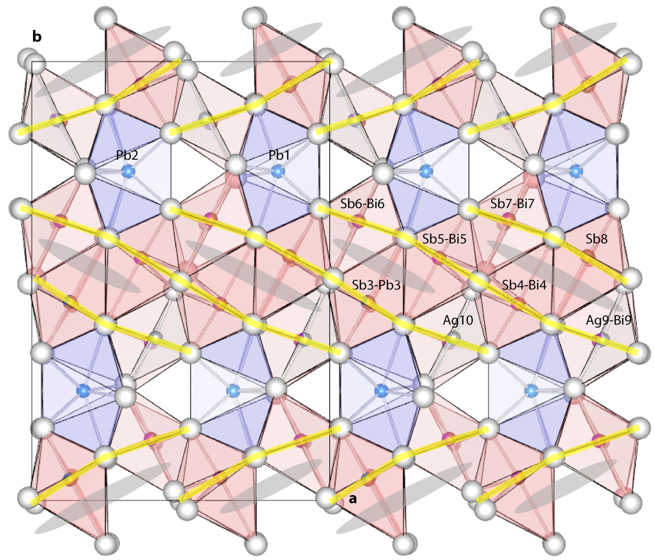

Figure 8. The orientation of the planes referenced by the in-plane and out-of-plane categories in the crystal structure of lazerckerite (thick yellow lines). The planes are predominantly aligned to the [001] zone axis and parallel to the lone electron pair micelles (grey ellipses). White spheres represent sulfur atoms. Blue polyhedra are bicapped trigonal prisms of Pb, and the red ones are octahedra. Figure 8 was created with VESTA (Momma and Izumi, 2011).

the out-of-plane bond pairs are oriented approximately perpendicular to the in-plane pairs and encompass the distances to the apical ligands. The graphical representation of these categories is provided in Fig. 7 for clarity.

In lazerckerite, the orientation of the "planes" typically aligns with [001], with deviations from the zone axis ranging from 0.1 to 5.8°, as illustrated in Fig. 8. The pairs of opposing bonds in Sb-bearing coordination polyhedra of lazerckerite are listed in Table 8. The graphical representation of the bond pairs, plotted against the element-specific bond-length hyperbolae for Sb (Berlepsch et al., 2001b), Bi (Topa et al., 2003), and Pb (Topa, 2001), is shown in Fig. 9. Except for Sb8, which closely aligns with the Sb hyperbola, the remaining Sb sites exhibit mixed positions and predominantly fall between the hyperbolae or in proximity to the hyperbola associated with the dominant element within the site population (e.g. Sb6–Bi6, Sb7–Bi7). The most noteworthy departure from this trend is observed in the bond pair S11-M4-S12 of Sb4–Bi4, likely attributed to its unusual sevenfold coordination caused by the split S9 position.

Armbruster and Hummel (1987) developed a very simple discriminating diagram which uses the average distance calculated for the three shortest Me–S bonds plotted against the average distance of the next two shortest bonds. The diagram

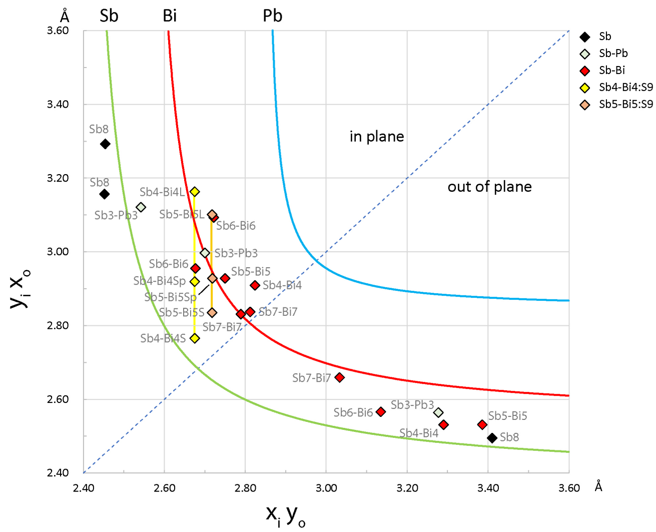

Figure 9. Bond pairs within the Sb-bearing octahedra found in the crystal structure of lazerckerite. Additionally, the diagram includes the sevenfold coordinations of Sb4–Bi4 and Sb5–Bi5, featuring the split S9 position. Sb4–Bi4L represents the in-plane bond pair for the longer distance to S9, while Sb4–Bi4S refers to the bond pair encompassing the shorter distance to S9. Sb4–Bi4Sp denotes the bond pair calculated for a theoretical, unsplit S9 position. The same nomenclature is applied to Sb5–Bi5. The deviation of data points from the median diagonal indicates increasing asymmetry of the opposing bonds.

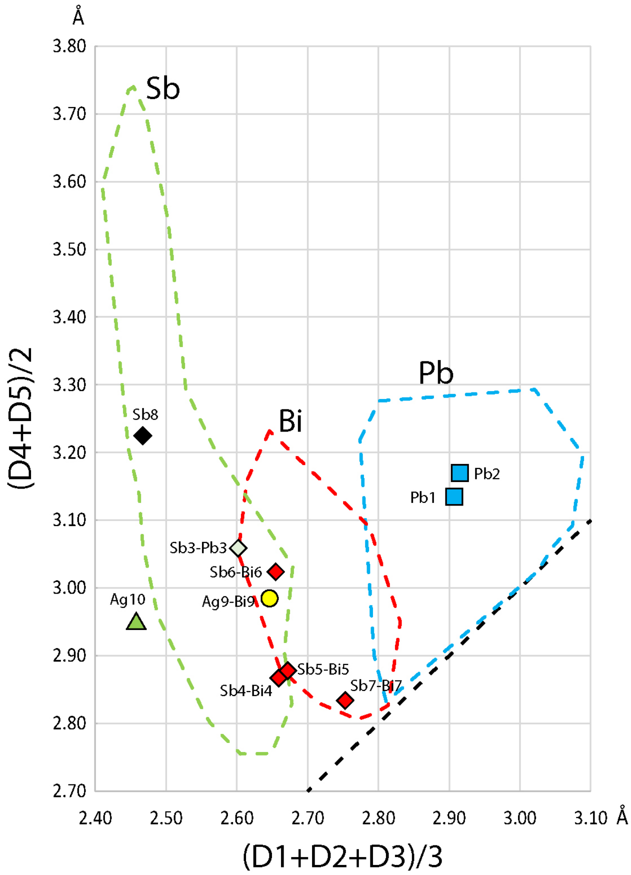

Figure 10. The Armbruster–Hummel diagram modified for the chemical content of lazerckerite. The element-specific fields have been delineated using data from more than 1300 coordination polyhedra in sulfosalts (Gheorghe Ilinca, personal communication, 2023), a notably larger dataset than the one employed in the original paper. The dotted diagonal black line in the diagram corresponds to regular polyhedra where the two mean values are equal. The bond lengths in ascending order are denoted as D1, D2, D3, D4, and D5.

for lazerckerite is illustrated in Fig. 10 and confirms the site populations suggested in the present work. The utilization of EDEV, representing the deviation of ECoN from the constrained coordination number, serves as a valuable metric for evaluating the internal distortion of coordination polyhedra and verifying the assignment of site populations. This approach is grounded in the observation that distinct EDEV values are characteristic of different central atoms or mixed sites (Ilinca, 2022). Table 9 and Fig. 11 present a comparison between the general average EDEV values and ranges for Pb, Bi, Sb, and Ag and mixtures within six-, seven-, and eightfold coordinations in over 170 sulfosalt crystal structures (Ilinca, 2022). These comparisons are juxtaposed with the specific EDEV values identified in lazerckerite. Overall, the opposing bond pairs, the ratios of bond-length averages and the state of EDEV confirm the site population assignments refined for the crystal structure of lazerckerite.

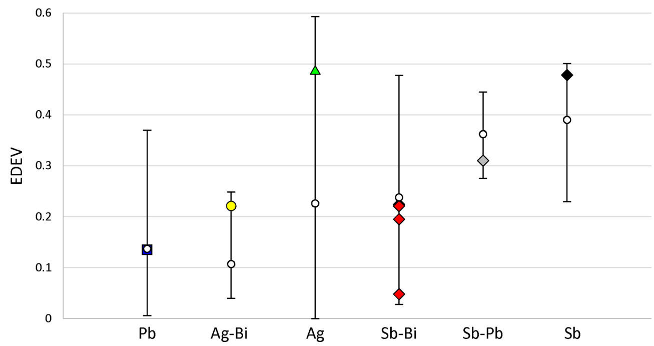

Figure 11. The plot of EDEV values in lazerckerite (coloured symbols) against the averages (white circles) and ranges (vertical bars) for over 170 sulfosalt crystal structures (Ilinca, 2022).

7 Relation to other species

Based on the current X-ray study we conclude lazerckerite belongs to the group of lillianite homologues with the unit cell type A ($a \approx 19$, $b \approx 13$, $c \approx 8.5$, $\beta \approx 90.1°$, $V \approx 2200$ in various cell settings; Table 10), such as fizelyite, ramdohrite, uchucchacuaite, menchettite, holubite, and oscarkempffite. Lazerckerite displays some similarity to oscarkempffite, although with several differences (we discuss only octahedral sites where all substitutions occur in lazerckerite): (1) the marginal octahedral (Sb,Bi) mixed site (called Sb1) in oscarkempffite (Topa et al., 2016) is the (Sb,Bi) mixed sites $M6$ and $M7$ in lazerckerite; (2) the marginal Ag sites in oscarkempffite become a pure Ag site (Ag10) and an (Ag,Bi) site $M9$ with (0.835Ag + 0.125Bi) in lazerckerite; and (3) two central octahedral sites in oscarkempffite – pure Sb site (Sb2) and (Sb,Bi) mixed site (called Sb3) – become a pure Sb site, two (Sb,Bi) mixed sites $M4$ and $M5$, and an (Sb,Pb) mixed site $M3$ with (0.64Sb + 0.36Pb). Bond distances of (Sb,Bi) sites in oscarkempffite are very similar to those in lazerckerite. The referred to oscarkempffite structure is the orthorhombic structure published in Topa et al. (2016).

Lazerckerite is a recent addition to the lillianite group, belonging to Strunz class 02.JB.40a and Dana class 3.04.15. It belongs to the mixed Sb–Bi members of the lillianite homologous series, which represents a fairly new and a not-so-frequent group among either Bi-dominant (lillianite branch) or Sb-dominant (andorite branch) members of the series. To this date, it is comprised of four minerals: terrywallaceite, oscarkempffite, clino-oscarkempffite, and staročeskéite. The recent discovery of lazerckerite and holubite (Pažout et al., 2023a) expands this subgroup.

Comparative parameters of all mixed Sb–Bi members and several Sb members for the characterization of lillianite homologues with $N = 4$, calculated from results of EPMA, are in Table 10. Figure 12 can serve as a practical tool for EPMA-equipped mineralogists who encounter Sb–Bi mixed phases. It shows the differences in the chemical composition (Bi/(Bi+Sb) vs. $L\%$) of individual mixed Sb–Bi mem-

Table 8. Opposing bond pairs in Sb-bearing polyhedra of lazerckerite.

Central atom	x_i [Å]	y_i [Å]	S–Me–S angle [°]	Position relative to the plane	Opposing ligands	Plane to [0 0 1] angle [°]
Sb3–Pb3	2.700	2.997	169.1	IP	S7 S10	5.8
	2.542	3.121	169.1	IP	S7 S4	
	2.564	3.277	178.2	OOP	S11 S1	
Sb4–Bi4	2.824	2.909	176.7	IP	S11 S12	0.6
	2.682	2.919	175.7	IP	S2 S9[a]	
	2.682	2.765	168.2	IP	S2 S9[b]	
	2.682	3.163	170.1	IP	S2 S9[c]	
	2.531	3.290	175.7	OOP	S10 S5	
Sb5–Bi5	2.759	2.922	177.6	IP	S11 S12	0.5
	2.725	2.919	174.5	IP	S2 S9[a]	
	2.725	2.835	165.3	IP	S2 S9[b]	
	2.725	3.101	171.8	IP	S2 S9[c]	
	2.531	3.386	174.6	OOP	S4 S6	
Sb6–Bi6	2.722	3.093	177.0	IP	S1 S2	0.1
	2.677	2.955	176.1	IP	S13 S11	
	2.566	3.135	172.9	OOP	S7 S8	
Sb7–Bi7	2.812	2.837	167.9	IP	S10 S5	1.6
	2.789	2.831	167.5	IP	S4 S6	
	2.659	3.033	178.8	OOP	S12 S3	
Sb8	2.454	3.293	177.4	IP	S10 S7	1.6
	2.452	3.157	174.6	IP	S4 S7	
	2.495	3.410	175.0	OOP	S2 S13	

[a] Distance to unsplit S9 (approximated as special position). [b] Shorter distance to S9. [c] Longer distance to S9. IP – in plane; OOP – out of plane.

Table 9. Average and range of EDEV in sulfosalts, compared with the actual values in lazerckerite.

	General EDEV*			
	Average	Min	Max	Lazerckerite
Pb (VIII)	0.137	0.006	0.369	0.135, 0.135
Ag,Bi (VI)	0.107	0.040	0.248	0.221
Ag (VI)	0.226	0.000	0.593	0.488
Sb–Bi (VI,VII)	0.238	0.028	0.477	0.048, 0.195, 0.224, 0.221
Sb–Pb (VI)	0.362	0.275	0.445	0.310
Sb (VI)	0.390	0.231	0.501	0.478

2mm* Based on a dataset of over 170 sulfosalt crystal structures (Ilinca, 2022); roman numerals denote the coordination number.

bers of the lillianite homologous series with $N = 4$ from the Staročeské pásmo Lode, Kutná Hora, Czech Republic. This graph includes all mixed Sb–Bi members known to this day with the exception of oscarkempffite and clino-oscarkempffite, which have so far not been identified in the Kutná Hora ore district. The distribution of unit cell types (discussed below) in the space of mixed Sb–Bi members of the lillianite homologous series is shown in Fig. 13, and the explanation of unit cell types is given in Table 11. A comparison of selected data for lazerckerite, quantrandorite, terrywallaceite, and oscarkempffite is given in Table 12.

Table 10 shows that for $L \approx 70\,\%$ there are four distinct mineral species that differ only in Bi content. Pure antimony members are ramdohrite (Makovicky et al., 2013) and fizelyite (Moëlo et al., 1984). When the Bi content substituting for Sb rises to $Bi/(Bi+Sb) = 0.26$–0.32, Bi prevails in two atomic positions (Bi4 and $M5$) while preserving the cell and symmetry of ramdohrite (unit cell type A), and the mineral becomes holubite. When the Bi content rises even further to 0.45, the cell and symmetry changes to that of orthorhombic lillianite (unit cell type B), and the mineral becomes staročeskéite (Pažout and Dušek, 2010; Pažout and Sejkora, 2018).

Similarly for $L \approx 90\,\%$, there are four mineral species. The pure antimony member is quatrandorite (unit cell type D) (Nespolo et al., 2012). When the Bi content rises to $Bi/(Bi+Sb) = 0.30$, the cell changes to unit cell type A, and the mineral becomes lazerckerite. When the Bi content rises to $Bi/(Bi+Sb) = 0.40$–0.45, the cell changes to unit cell type C, and the mineral becomes terrywallaceite (Pažout and Dušek, 2009; Yang et al., 2013). A further increase in Bi does not change the cell and symmetry. This holds true

Table 10. Comparative parameters for the characterization of mixed Sb–Bi members of the lillianite homologues with $N = 4$ calculated from results of EPMA. Included are all mixed Sb–Bi members and several Sb members.

Mineral	N^a	$L\%^a$	Bi/(Bi+Sb)^a	Unit cell type	S.G.	Ref.
Holubite	4–4.4	64–75	0.26–0.36	A	$P2_1/n$	1
Ramdohrite	4–4.4	68–75	0	A	$P2_1/n$	2
Fizélyite	3.9–4.2	58–62	0	A	$P2_1/n$	3
Ag-excess fizélyite	4.2–4.8	62–70	0	A	$P2_1/n$	4
Staročeskéite	3.9–4.2	65–75	0.45–0.55	B	*Cmcm*	5, 6
Quatrandorite	3.9 - 4.2	90 - 95	0	D	$P2_1/c$	7
Lazerckerite	4–4.4	90–95	0.28–0.38	A	$P2_1/c$	
Senandorite	3.9–4.2	98–102	0	E	$Pn2_1a$	8
Terrywallaceite	3.9–4.2	80–112	0.45–0.75	C	$P2_1/c$	9, 10
Gustavite	3.9–4.2	64–104	0.75–1	C	$P2_1/c$	11
Oscarkempffite	4–4.1^b	120–124^b	0.29–0.37^b	A	*Pnca*^{c}	12
Clino-oscarkempffite	4–4.2^b	122–123^b	0.48^b	F	$P2_1/c$	13

N – order of the lillianite homologue. $L\%$ – degree of the $Ag^+ + (Bi,Sb)^{3+} \leftrightarrow 2\,Pb^{2+}$ substitution. Bi/(Bi+Sb) – degree of $Sb^{3+} \leftrightarrow Bi^{3+}$ substitution (0 for pure antimony members). [a] Values encountered by EPMA (Pažout, 2017). [b] Values in Ref. 12 or 13, respectively. [c] Later attempts to improve the structure revealed $P2_1/n$ as possible S.G. (Dan Topa, personal communication, 2024). References: (1) Pažout et al. (2023a); (2) Makovicky et al. (2013); (3) Moëlo et al (1984); (4) Yang et al. (2009); (5) Pažout and Dušek (2010); (6) Pažout and Sejkora (2018); (7) Nespolo et al. (2012); (8) Sawada et al. (1987); (9) Pažout and Dušek (2009); (10) Yang et al. (2013); (11) Makovicky and Topa (2011); (12) Topa et al. (2016); and (13) Makovicky et al. (2017).

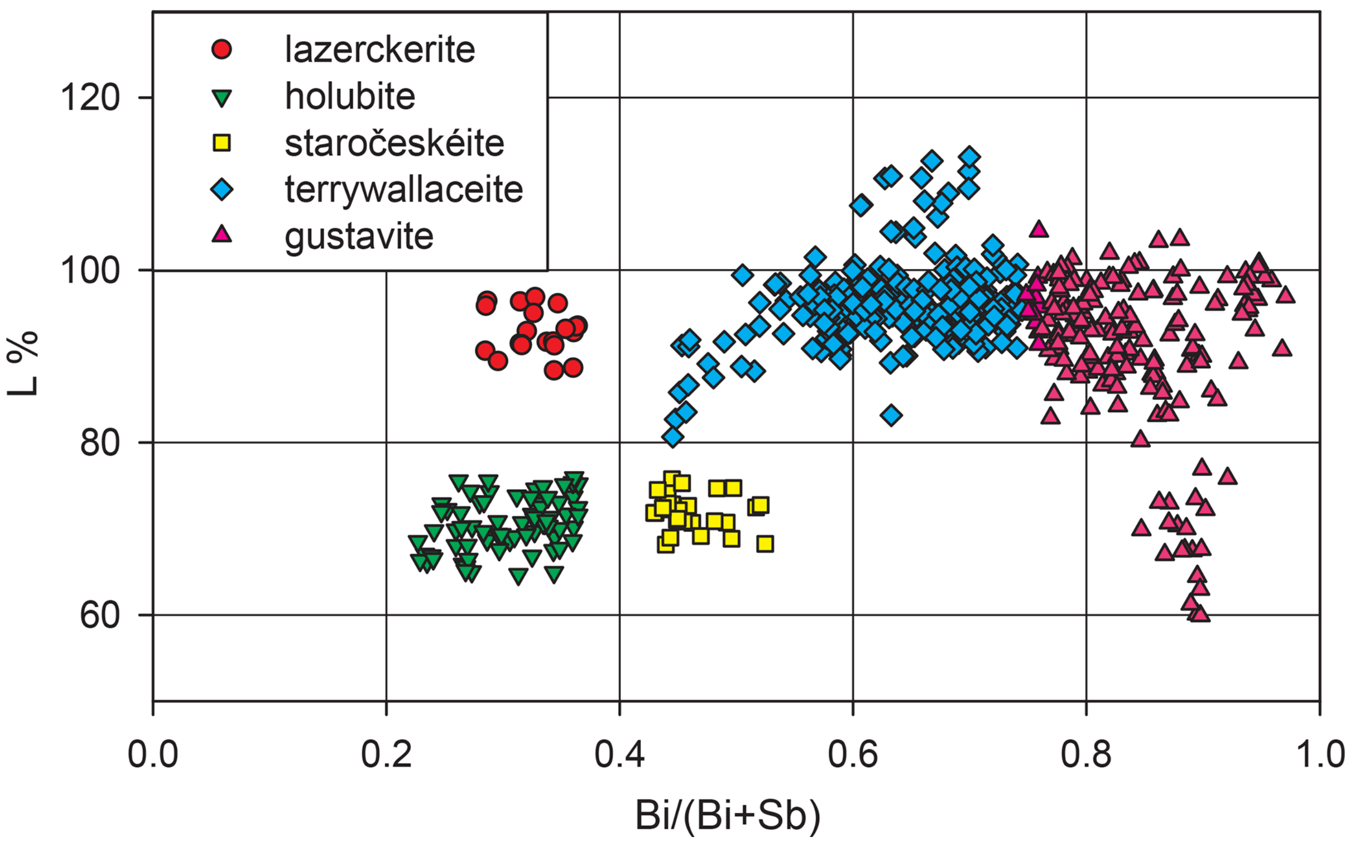

Figure 12. Chemical composition (Bi/(Bi+Sb) vs. $L\%$) of Sb–Bi mixed members of the lillianite homologous series with $N = 4$ from the Staročeské pásmo Lode, Kutná Hora, Czech Republic. Analytical points with gustavite composition (violet triangles) below $L = 75\,\%$ should be checked by single-crystal diffraction since they may show unit cell type C of gustavite or unit cell type B of lillianite (Pažout, 2017; see Fig. 13).

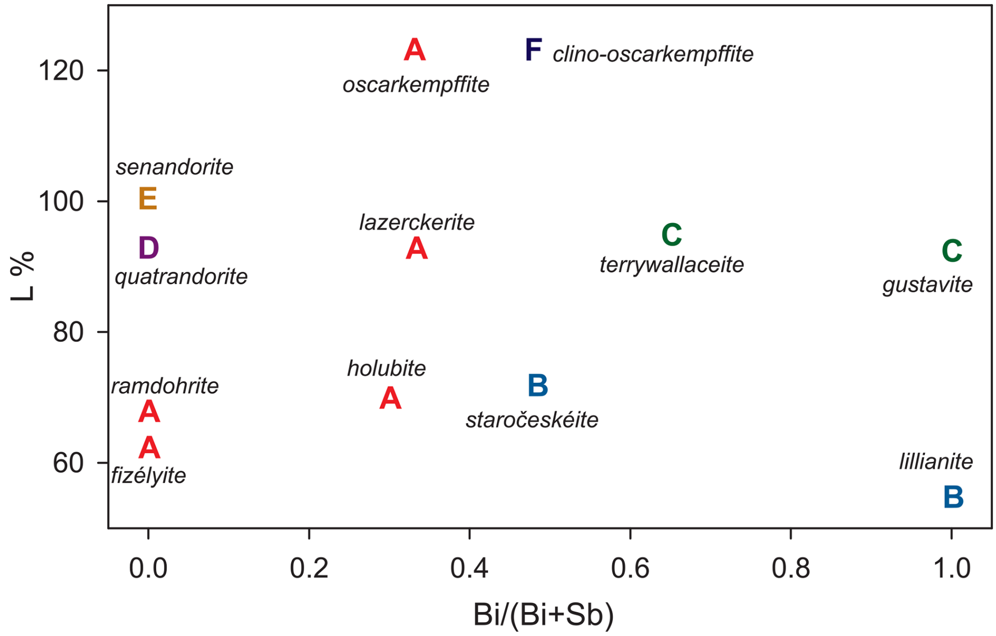

Figure 13. Distribution of unit cell types in the space of mixed Sb–Bi members of the lillianite homologous series; for explanation see Table 11.

Table 11. Unit cell types of Bi- and Sb-bearing lillianite homologues according to sizes of unit cell parameters [in Å and degrees] and cell volumes [Å^3] regardless of axial setting, simplified (approximated) to highlight parameter and volume multiples.

A	$a \approx 19$	$b \approx 13$	$c \approx 8.5$	$\beta \approx 90°$	$V \approx 2200$
B	$a \approx 19$	$b \approx 13$	$c \approx 4.25$		$V \approx 1100$
C	$a \approx 19$	$b \approx 7$	$c \approx 8.5$	$\beta \approx 107°$	$V \approx 1100$
D	$a \approx 19$	$b \approx 13$	$c \approx 17$	$\beta \approx 90°$	$V \approx 4200$
E	$b \approx 19$	$a \approx 13$	$c \approx 25.5$		$V \approx 6300$
F	$b \approx 19$	$a \approx 40$	$c \approx 8.5$	$\beta \approx 96°$	$V \approx 6300$

up to Bi/(Bi+Sb) = 0.75, when Bi becomes prevalent in all three (Sb,Bi) metal positions, and the mineral becomes gustavite while keeping the cell and symmetry of terrywallaceite (unit cell type C). Thus gustavite is defined as a mineral with Bi =(Bi+Sb) from 1 (pure bismuthian gustavite with no antimony) to 0.75 (Sb-rich gustavite).

Now if we have the Bi content constant and change the L%, the situation is as follows: for example for Bi/(Bi+Sb) ≈ 0.5, the mineral with $L = 100\,\%$ is terrywallaceite (unit cell type C) with the cell and symmetry of gustavite. If the L% decreases (i.e. Pb rises and Ag + (Bi,Sb) decreases) to $L \approx 70\,\%$, the monoclinic cell changes to an orthorhombic cell of lillianite (unit cell type B), and the mineral becomes staročeskéite. If on the other hand L rises to 125 % (which is the case of the Peruvian ore district of Julcani but which is not so in Europe – not even in Kutná Hora, certainly due to different formation conditions of Andean deposits and omnipresent Pb in formation fluids in Kutná Hora), the mineral becomes clino-oscarkempffite (unit cell type F) with a uniquely tripled ∼ 13.3 Å parameter (Makovicky et al., 2017).

Staying with the constant Bi content, for Bi/(Bi+Sb) ≈ 0.3 there are three distinct mineral species, differing only in L%, with all three minerals having the same cell type and symmetry. Starting from the Pb-richer end, the mineral with $L = 70\,\%$ is holubite. If the Ag and (Bi,Sb) contents rise and Pb drops so that $L = 90\,\%$, the mineral becomes lazerckerite. While the two minerals have the same cell type and symmetry, the differences in structures are eye-catching. While in holubite there are only pure Sb sites and one pure bismuth site, in lazerckerite there are multiple (Sb,Bi) mixed sites similar to oscakempffite (Topa et al., 2016) or clino-oscarkempffite (Makovicky et al., 2017). If the Pb content drops even further and Ag + (Bi,Sb) rises even more to the over-substitution of $L = 120\,\%$ (the over-substitution can be achieved only by replacing the trigonal prismatic Pb by Ag and (Bi,Sb)), the mineral becomes oscakempffite with the same cell and symmetry.

Thus, lazerckerite stands as a unique mineral species both structurally and chemically, distinctly differing from quatrandorite, terrywallaceite, oscarkempffite, holubite, and staročeskéite. It is defined as a lillianite homologue with the following three requirements: $N = 4$, L ($Ag^+ + (Bi^{3+},Sb^{3+}) \leftrightarrow 2\ Pb^{2+}$ substitution) ≈ 90 %–95 %, and about one-third of atom percentage of antimony is replaced by bismuth (Bi/(Bi+Sb) ≈ 0.30–0.38). The mineral phases with this N and L% but Bi/(Bi+Sb) below 0.20 should be in lack of single-crystal data classified as Bi-rich

Table 12. Comparative data for lazerckerite and related minerals.

	Lazerckerite	Oscarkempffite	Quatrandorite	Terrywallaceite
Locality	Kutná Hora, Czechia	Potosi, Bolivia	San Jose, Bolivia	Julcani, Peru
Reference	this proposal	Topa et al. (2016)	Nespolo et al. (2012)	Yang et al. (2013)
Ideal composition	$Ag_{3.75}Pb_{4.5}(Sb_{7.75}Bi_4)_{\Sigma 11.75}S_{24}$	$Ag_{10}Pb_4Sb_{17}Bi_9S_{48}$	$Ag_{3.75}Pb_{4.5}Sb_{11.75}S_{24}^{*}$	$AgPb(Sb,Bi)_3S_6$
Empirical composition	$(Ag_{3.61}Cu_{0.04})_{\Sigma 3.65}(Pb_{4.54}Fe_{0.02}Cd_{0.01})_{\Sigma 4.57}$ $(Sb_{7.87}Bi_{3.75})_{\Sigma 11.62}(S_{24.14}Se_{0.01})_{\Sigma 24.15}$	$Ag_{9.92}Cu_{0.24}Pb_{4.00}Sb_{17.36}$ $Bi_{8.64}S_{47.84}$	$Ag_{3.6}Cu_{0.2}Pb_{4.2}$ $Fe_{0.1}Sb_{11.5}As_{0.4}S_{24}$	$Ag_{1.02}Pb_{0.87}(Sb_{1.53}Bi_{1.47})_{\Sigma 3.00}$ $(S_{5.94}As_{0.06})_{6.00}$
Space group	$P2_1/c$	*Pnca*	$P2_1/c$	$P2_1/c$
a	13.2083(9)	8.2939(12)	19.1686 (19)	6.9764(4)
b	19.4595(8)	13.1991(19)	17.160 (3)	19.351(1)
c	8.4048(13)	19.332(3)	13.042	8.3870(4)
β	90.032(7)	90	90.008 (12)	107.519(2)
V	2160.3(4)	2116.3(5)	4289.9 (11)	1079.7(1)
Z	2	1	4	4
Strongest lines	3.4071/34[a]	3.663/30[b]	3.436/59[a]	3.680/23[b]
In XRD	3.353/100	3.354/100	3.305/100	3.369/100
Powder	2.9023/39	2.988/40	2.909/74	3.010 /33
Pattern	2.9009/37	2.889/80	2.755/45	2.911 /58

[a] Calculated from the structure data. [b] Measured powder X-ray data. * Moëlo et al., 1989.

quatrandorite and the compositions with Bi/(Bi+Sb) above 0.45 as terrywallaceite.

If we look at how to evaluate samples from Kutná Hora with border values of Bi/(Bi+Sb), which for lazerckerite with $L\% \approx 90$–95 are 0.28 and 0.46 (values encountered by EPMA by the first author of this article), we can conclude that the value of 0.28 still corresponds in all cases to lazerckerite, no matter in which of the five bismuth mixed sites the depletion of Bi occurs. Analytical points with the values between 0.40 and 0.46 are difficult to classify because these overlap with the substitution field of terrywallaceite. In the case of a mineral with multiple bismuth mixed sites (four (Bi,Sb) mixed sites and one (Ag,Bi) mixed site in lazerckerite and three (Bi,Sb) mixed sites in terrywallaceite), it is hard to speculate on how the increase in Bi will show in individual sites.

While the upper limit for terrywallaceite was deduced by Yang et al. (2013) at about Bi/(Bi+Sb) = 0.75 (thus the Sb-rich gustavite of Pažout and Dušek, 2009, with Bi/(Bi+Sb) = 0.70 is in fact terrywallaceite), the lower limit is less obvious. Terrywallaceite of Yang et al. (2013) has Bi/(Bi+Sb) = 0.49, and even if only the central octahedral sites $M2$ (0.60Bi + 0.40Sb) and $M3$ (0.95Sb + 0.05Bi) are considered for Sb for Bi substitution, it still has a space for an increase in Sb (0.1 apfu in $M2$ and 0.05 apfu in the $M3$). Such a composition (0.50Bi + 0.50Sb in $M2$ and only Sb in $M3$) has Bi/(Bi+Sb) equal to 0.44. Since some increase in Sb in the marginal octahedral site $M1$ site (0.82Bi + 0.18Sb) of Yang et al. (2013) cannot be ruled out and also since the antimony content in the $M2$ site may climb over 50 %, it is reasonable to consider all composition above Bi/(Bi+Sb) = 0.40 to belong to terrywallaceite or to constitute a mixture (intergrowth) of terrywallaceite and lazerckerite. A definitive answer of which mineral a particular composition belongs to would be given by single-crystal diffraction, which should show the $a \approx 19$, $b \approx 13$, $c \approx 8.5$, $\beta \approx 90°$, and $V \approx 2200$ cell of lazerckerite or the $a \approx 19$, $b \approx 7$, $c \approx 8.5$, $\beta \approx 107°$, and $V \approx 1100$ cell of terrywallaceite.

Comparing the data from Kutná Hora with published data from elsewhere in the past, it is possible that a mineral phase corresponding to lazerckerite has been found before as Keutsch and Brodtkorb (2008) described samples from Oruro, Bolivia, with $L\% = 94.4$ and Bi/(Bi+Sb) = 0.23, which may correspond to lazerckerite.

Data availability. Crystallographic data of lazerckerite are available in the Supplement.

Supplement. The supplement related to this article is available online at: https://doi.org/10.5194/ejm-36-641-2024-supplement.

Author contributions. RP: discovery of the new mineral, conception of the project, locality research and preparation of samples, EPMA data interpretation, single-crystal X-ray data interpretation and structure solution, and writing of the paper with inputs from other authors. MD: single-crystal X-ray data interpretation. JS: optical measurements and preparation of article graphics. JP: sample extraction and single-crystal X-ray measurements. GI: coordination polyhedra and polyhedral distortion. ZD: EPMA measurements.

Competing interests. The contact author has declared that none of the authors has any competing interests.

Disclaimer. Publisher's note: Copernicus Publications remains neutral with regard to jurisdictional claims made in the text, published maps, institutional affiliations, or any other geographical representation in this paper. While Copernicus Publications makes every effort to include appropriate place names, the final responsibility lies with the authors.

Special issue statement. This article is part of the special issue "New minerals: EJM support". It is not associated with a conference.

Acknowledgements. We appreciate many constructive comments of the anonymous reviewers that helped to improve this paper significantly. The Institute of Physics of the Czech Academy of Sciences is thanked for providing access to their single-crystal X-ray diffraction laboratory. Dan Topa is thanked for the initial EPMA measurements

Financial support. This research has been supported by the Ministry of Culture of the Czech Republic (long-term project DKRVO 2024-2028/1.II.a; National Museum grant no. 00023272) and the Czech Science Foundation (GAČR project 15-18917S). The crystallographic experiment used the CzechNanoLab Research Infrastructure supported by MEYS CR (grant no. LM2023051).

Review statement. This paper was edited by Segrey Krivovichev and reviewed by three anonymous referees.

References

Armbruster, T. and Hummel, W.: (Sb,Bi,Pb) ordering in sulfosalts: Crystal-structure refinement of a Bi-rich izoklakeite, Am. Mineral., 72, 821–831, 1987.

Berlepsch, P., Makovicky, E., and Balić-Žunić, T. : Crystal chemistry of meneghinite homologues and related sulfosalts, Neues Jb. Miner. Monat., 2001, 115–135, 2001a.

Berlepsch, P., Makovicky, E., and Balić-Žunić, T.: Crystal chemistry of sartorite homologues and related sulfosalts, Neues Jb. Miner. Abh., 176, 45–66, 2001b.

Holub, M., Hoffman, V., Mikuš, V., and Trdlička, Z.: Polymetallic mineralization of the Kutná Hora ore district, Sborník geologických věd, ložisková geologie, Mineralogie, 23, 69–123, 1982 (in Czech).

Ilinca, G.: Charge Distribution and Bond Valence Sum Analysis of Sulfosalts. The ECoN21 computer program, Minerals, 12, 924, https://doi.org/10.3390/min12080924, 2022.

Keutsch, F. and Brodtkorb, M. K.: Metalliferous paragenesis of the San José mine, Oruro, Bolivia, J. S. Am. Earth Sci., 25, 485–491, 2008.

Makovicky, E. and Topa, D.: The crystal structure of gustavite, PbAgBi3S6, Analysis of twinning and polytypism using the OD approach, Eur. J. Mineral., 23, 537–550, https://doi.org/10.1127/0935-1221/2011/0023-2114, 2011.

Makovicky, E. and Topa, D.: Lillianites and andorites: new life for the oldest homologous series of sulfosalts, Mineral. Mag., 78, 387–414, 2014.

Makovicky, E., Mumme, W. G., and Gable, R. W.: The crystal structure of ramdohrite, $Pb_{5.9}Fe_{0.1}Mn_{0.1}In_{0.1}Cd_{0.2}Ag_{2.8}Sb_{10.8}S_{24}$: A new refinement, Am. Mineral., 98, 773–779, 2013.

Makovicky, E., Topa, D., and Paar, W. H.: The definition and crystal structure of clino-oscarkempffite, $Ag_{15}Pb_6Sb_{21}Bi_{18}S_{72}$, Eur. J. Mineral., 30, 569–579, https://doi.org/10.1127/ejm/2017/0029-2688, 2017.

Malec, J. and Pauliš, P.: Kutná Hora ore mining district and appearances of past mining and metallurgic activities on its territory. Bulletin Mineralogicko-petrologického oddělení Národního muzea v Praze, 4/5, 86–105, 1997 (in Czech with English abstract).

Moëlo, Y., Makovicky, E., and Karup-Møller, S.: New data on the minerals of the andorite series, Neues Jhb. Miner. Monat., 4, 175–182, 1984.

Moëlo, Y., Makovicky, E., and Karup-Møller, S: Sulfures complexes plombo-argentiferes: mineralogie et cristallochimie de la serie andorite-fizelyite (Pb,Mn,Fe,Cd,Sn)3-$2x$(Ag,Cu)x(Sb,Bi,As)$2+x$(S,Se)$_6$, Documents du Bureau de Recherches Geologiques et Mineres, No. 167, Editions du BRGM, Orleans, France, 107 pp., 1989 (in French).

Momma, K. and Izumi, F.: VESTA 3 for three–dimensional visualization of crystal, volumetric, and morphology data, J. Appl. Crystall., 44, 1272–1276, 2011.

Nespolo, M., Ozawa, T., Kawasaki, Y., and Sugiyama, K.: Structural relations and pseudosymmetries in the andorite homologous series, J. Miner. Petrol. Sci., 107, 226–243, 2012.

Palatinus, L. and Chapuis, G.: Superflip – a computer program for the solution of crystal structures by charge flipping in arbitrary dimensions, J. Appl. Crystall., 40, 786–790, 2007.

Pažout, R.: Lillianite homologues from Kutná Hora ore district, Czech Republic: a case of large-scale Sb for Bi substitution, J. Geosci., 62, 37–57, 2017.

Pažout, R. and Dušek, M.: Natural monoclinic $AgPb(Bi_2Sb)_3S_6$, an Sb-rich gustavite, Acta Crystallogr., C65, i77–i80, 2009.

Pažout, R. and Dušek, M.: Crystal structure of natural orthorhombic Ag0.71Pb1.52Bi1.32Sb1.45S6, a lillianite homologue with $N=4$; comparison with gustavite, Eur. J. Mineral., 22, 741–750, 2010.

Pažout, R. and Sejkora, J.: Staročeskéite, $Ag_{0.70}Pb_{1.60}(Bi_{1.35}Sb_{1.35})\Sigma 2.70S_6$, from Kutná Hora, Czech Republic, a new member of lillianite homologous series, Mineral. Mag., 82, 993–1005, 2018.

Pažout, R., Sejkora, J., and Šrein, V.: Bismuth and bismuth–antimony sulfosalts from Kutná Hora vein Ag–Pb–Zn ore district, Republic, J. Geosci., 62, 59–76, 2017.

Pažout, R., Plášil, J., Dušek, M., Sejkora, J., and Dolníček, Z.: Holubite, $Ag_3Pb_6(Sb_8Bi_3)\Sigma 11S_{24}$, from Kutná Hora, Czech Republic, a new member of the andorite branch of the lillianite homologous series, Mineral. Mag., 87, 582–590, https://doi.org/10.1180/mgm.2023.34, 2023a.

Pažout, R., Plášil, J., Dušek, M., Sejkora, J., and Ilinca, G.: Lazerckerite, IMA 2022-113, CNMNC Newsletter 72, Mineral. Mag., 87, 512–518, https://doi.org/10.1180/mgm.2023.21, 2023b.

Petříček, V., Dušek, M., Plášil, J., and Palatinus, L.: Jana2020 – a new version of the crystallographic computing system Jana, Z. Kristallogr., 229, 345–352, https://doi.org/10.1515/zkri-2023-0005, 2023.

Pouchou, J. L. and Pichoir, F.: "PAP" ($\varphi\rho Z$) procedure for improved quantitative microanalysis, in: Microbeam Analysis, edited by: Armstrong, J. T., San Francisco Press, San Francisco, 104–106, 1985.

Putz, H. and Brandenburg, K.: Diamond – Crystal and Molecular Structure Visualization, Crystal Impact-GbR, Kreuzherrenstr. 102, 53227 Bonn, Germany, 2017.

Rigaku: CrysAlis CCD and CrysAlis RED, Rigaku – Oxford Diffraction Ltd, Yarnton, Oxfordshire, UK, 2019.

Sawada, H., Kawada, I., Hellner, E., and Tokonami, M.: The crystal structure of senandorite (andorite VI): PbAgSb3S6, Z. Kristallogr., 180, 141–150, 1987.

Topa, D.: Mineralogy, Crystal Structure and Crystal Chemistry of the Bismuthinite–Aikinite Series from Felbertal, Austria, Ph.D. thesis, Institute of Mineralogy, University of Salzburg, Austria, 2001.

Topa, D., Makovicky, E., and Balić–Žunić, T.: Crystal structures and crystal chemistry of members of the cuprobismutite homologous series of sulfosalts, Can. Mineral., 41, 1481–1501, 2003.

Topa, D., Paar, W. H., Makovicky, E., Stanley, C. J., and Roberts, A. C.: Oscarkempffite, $Ag_{10}Pb_4(Sb_{17}Bi_9)\Sigma 26S_{48}$, a new Sb–Bi member of the lillianite homologous series, Mineral. Mag., 80, 809–817, https://doi.org/10.1180/minmag.2016.080.024, 2016.

Trömel M.: Empirische Beziehungen zur Sauerstoffkoordination um Antimon(lll) und Tellur(lV) in Antimoniten und Telluriten, J. Solid State Chem., 35, 90–98, 1980.

Yang, H., Downs, R. T., Burt, J. B., and Costin, G.: Structure refinement of an untwinned single crystal of Ag-excess fizelyite, $Ag_{5.94}Pb_{13.74}Sb_{20.84}S_{48}$, Can. Mineral., 47, 1257–1264, 2009.

Yang, H., Downs, R. T., Evans, S. H., and Pinch, W. W.: Terrywallaceite, $AgPb(Sb,Bi)3S_6$, isotypic with gustavite, a new mineral from Mina Herminia, Julcani Mining District, Huancavelica, Peru, Am. Mineral., 98, 1310–1314, 2013.